RESEARCH ARTICLE

ADVANCED MATERIALS INTERFACES Open Access

www.advmatinterfaces.de

Selective Transparent Contacts Based on a Hafnium-Titanium Oxide Alloy with Optimized Band Alignment for c-Si Solar Cells

Charif Tamin, Céline Chevalier, Anil Kumar Bharwal,* Claude Botella, Thomas Fix, Alain Fave, and Erwann Fourmond*

In this study, the potential of hafnium-titanium oxide ($Hf_xTi_{1-x}O_y$, HTO) thin films is explored and deposited by low-temperature (75 °C) atomic layer deposition (ALD) as selective contacts for crystalline silicon (c-Si) solar cells. Through a comprehensive analysis of their selectivity, optical and chemical properties, and band alignment characteristics, the HTO films are shown to exhibit remarkable electron selectivity. They formed efficient ohmic contacts on n-type silicon, while exhibiting diode-like characteristics on p-type silicon, confirming their selective behavior. Band alignment analysis at the HTO/n-Si interface revealed a high valence band offset and a low conduction band offset, facilitating efficient electron extraction and blocking hole transport. Optical measurements demonstrate the high optical transparency of the HTO films with a bandgap above 3.5 eV, making them suitable for photovoltaic applications. A proof-of-concept photovoltaic device is evaluated, and significant improvements are observed in all solar cell parameters following the incorporation of HTO, highlighting the potential of low-temperature ALD-deposited HTO films as efficient electron-selective contacts for next-generation c-Si solar cells.

1. Introduction

Conventional crystalline silicon (c-Si) solar cell technologies use doped homojunctions to separate photogenerated charges.[1] This approach involves a high thermal budget, which is essential for creating highly doped regions in the c-Si for charge separation. In this configuration, the main losses are still associated with recombination at the c-Si/metal interfaces and bandgap narrowing in highly doped c-Si regions. These problems can be addressed using an innovative passivated contact strategy, which enables a single type of charge carrier (electrons or holes) to be collected with low resistance, and reduced recombination losses.

This concept has been implemented in silicon heterojunction (SHJ) solar cells, where thermal diffusion forms no heavily doped regions. Instead, different layers are applied on the silicon surface to passivate it and create selective contacts for a specific type of charge carrier. This approach has outperformed traditional c-Si solar cells, pushing efficiency to 26.81%, close to theoretical limits.[2] In these SHJ architectures, an ultrathin layer of intrinsic hydrogenated amorphous silicon is used as a passivation layer, combined with a doped silicon layer as a selective contact.[3,4] Although these contacts offer a superior performance, they still present a few limitations. These contacts involve dopants introduced by toxic gaseous processes, such as boron for p-type silicon and phosphorus for n-type silicon, via expensive techniques. In addition, these materials are not fully transparent, leading to parasitic optical losses.

Transition metal oxides (TMOs) have emerged as highly promising candidates for both hole- and electron-selective contacts in n- and p-type silicon solar cells.[5]

For hole-selective contacts, materials with a high work function (WF) are typically used, such as molybdenum oxide (MoO_x), tungsten oxide (WO_x), copper oxide (Cu_2O), vanadium oxide (VO_x), and nickel oxide (NiO_x).[6–12] Electron-selective contacts use low WF, such as zinc oxide (ZnO), tin oxide (SnO_2), and titanium dioxide (TiO_2).[13–16] Electron-selective TMOs are often combined with interfacial layers, such as lithium fluoride (LiF), to minimize the contact resistance at the interface between

C. Tamin, C. Chevalier, C. Botella
CNRS
Ecole Centrale de Lyon
INSA Lyon
Université Claude Bernard Lyon 1
CPE Lyon, INL, UMR5270, Villeurbanne 69100, France
E-mail: chariftamin@insa-lyon.fr

A. K. Bharwal, T. Fix
ICube Laboratory
University of Strasbourg and CNRS
Strasbourg 67037, France
E-mail: anilbharwal@gmail.com

A. Fave, E. Fourmond
INSA Lyon
Ecole Centrale de Lyon
CNRS
Université Claude Bernard Lyon 1
CPE Lyon, INL, UMR5270, Villeurbanne 69100, France

The ORCID identification number(s) for the author(s) of this article can be found under https://doi.org/10.1002/admi.202500083

© 2025 The Author(s). Advanced Materials Interfaces published by Wiley-VCH GmbH. This is an open access article under the terms of the Creative Commons Attribution License, which permits use, distribution and reproduction in any medium, provided the original work is properly cited.

DOI: 10.1002/admi.202500083

the TMOs and the metal contact.[17] This raises the question of whether the selectivity is due to the TMOs or to the interfacial layers. Several studies have shown that materials such as LiF are also electron selective and can be applied directly to c-Si(n) without TMOs.[3,18] A key challenge to achieve optimal band alignment and low contact resistance at the c-Si/metal interface without the need for additional interlayers is to fine-tune the properties of standard transition metal oxides (TMOs). Recently, a promising strategy of stacking different TMOs has been investigated by several research groups in the PV community. This approach allows tuning the optical and electronic properties of standard TMOs by using atomic layer deposition (ALD) in supercycle mode, which allows precise control over chemical composition and film thickness. This new approach paves the way for the exploration of new TMO combinations and provides a rich platform for the discovery of exotic alloys.

New $Al_xTi_{1-x}O_y$ alloys with alternating TiO_x and Al_2O_3 deposition have been exploited as selective contacts for c-Si solar cells.[19–22] Excellent electronic selectivity and surface passivation properties have been demonstrated with these alloys. A similar approach has also been used to tune the properties of NiO_x-based alloys by alternating NiO_x with ZnO and Al_2O_3, resulting in significantly improved hole selectivity.[12,23]

In this study, we developed a new alloying system by combining the deposition of hafnium oxide (HfO_2) and titanium oxide (TiO_2) using the ALD supercycle mode. This approach exploits the unique properties of TiO_2 and investigates the effect of Hf incorporation on the optical, electronic, and electrical properties of this alloy for potential application in all TMOs-based c-Si solar cells.

2. Results and Discussion

2.1. Chemical Characterization

X-ray photoelectron spectroscopy (XPS) characterization was performed on multi-supercycle hafnium-titanium oxide (HTO) films (≈7 nm thick) to investigate their bulk chemical composition, as well as on ultrathin HTO films (≈0.7 nm) with a single-supercycle to closely examine the interface with silicon. The core-level spectra of the films are presented in **Figure 1**.

The high-resolution Ti 2p spectra provided valuable information about the titanium oxidation states and bonding. For the thicker sample, two distinct peaks were observed: the first at 459.2 eV, corresponding to Ti $2p_{3/2}$, and the second at 465 eV, corresponding to Ti $2p_{1/2}$. In the thinner sample, these peaks shifted to higher energies, with Ti $2p_{3/2}$ at 459.5 eV and Ti $2p_{1/2}$ at a slightly higher energy. These values correspond to Ti(4+), as reported for titanium oxides (TiO_2).[24–27]

High-resolution spectra of Hf 4f were also present in both samples, even in the ultrathin sample, which contained only one Hf cycle during preparation. The Hf 4f spectra exhibited a characteristic doublet with peaks at approximately 17.6 eV for Hf $4f_{7/2}$ and 19.25 eV for Hf $4f_{5/2}$. In the thinner sample, these peaks also shifted to higher energies: 17.8 eV for Hf $4f_{7/2}$ and 19.4 eV for Hf $4f_{5/2}$. These values correspond to Hf(4+), as reported in the literature for haffinium oxyde (HfO_2).[28,29]

High-resolution spectra of O 1s were also analyzed in both the bulk and interface samples. In the bulk sample, a doublet was observed, with a dominant peak at 530.67 eV and an atomic concentration of ≈ 65%, corresponding to metal-oxygen bonds, specifically Ti-O and Hf-O. A less prominent secondary peak was observed at 532.09 eV, with an atomic concentration of ≈ 35%. At the interface, for the ultrathin film, the dominant peak shifted to 532.45 eV with an atomic concentration of ≈ 68%, indicating the presence of hydroxyl groups or oxygen-related defects.[27,30] The peaks around 532 eV can ve attributed to SiO_2 or hafnium silicate.[31–33] The secondary peak at the interface appeared around 530.1 eV, with an atomic concentration of ≈ 32%.

XPS analysis revealed that the chemical composition and oxidation states of the HTO films are consistent with Ti^{4+} and Hf^{4+} species. Shifts in the binding energies were observed at the silicon interface, indicating changes in the chemical environment and the presence of hydroxyl groups or oxygen-related defects.

2.2. Band Alignment

To determine the band alignment at the HTO/c-Si heterointerface, a series of measurements was conducted to characterize the optical properties, work function, and surface photovoltage (SPV) of the HTO films.

2.2.1. Optical Measurements

Ellipsometric measurements were performed on the samples grown on silicon wafers in the 1.4 – 5.9 eV spectral range. The dispersion formula used was based on the Tauc-Lorentz formula.[34] The model consisted of a single HTO layer on top of the c-Si substrate. The goodness-of-fit value (Chi-Square χ^2) was lower than 0.09 for both films HTO-5C and HTO 10C for a calculated thickness of 3.44 ± 0.03 and 6.99 ± 0.02 nm respectively. Figures S3 and S4 (Supporting Information) show the quality of the fit between the measured and simulated data, where $I_s = \sin(2\Psi)\sin(\Delta)$ and $I_c = \sin(2\Psi)\cos(\Delta)$. **Figure 2a** shows the n and k values for the films and Figure 2b the Tauc plot for an indirect bandgap material with an extracted bandgap value of 3.79 and 3.58 ±0.07 eV for HTO-5C and HTO-10C respectively. The choice of an indirect bandgap model is supported by the higher proportion of TiO_x in the films, which is known for its indirect bandgap nature, and the recent investigations by Shehata et al. on the different TMOs stacks.[22,35]

2.2.2. Work Function and Surface Photovoltage

Kelvin probe (KP) and SPV measurements were performed on HTO films and a clean n-type c-Si (HF-cleaned prior to measurement).

Figure 3a shows the dark WF of HTO films of different thicknesses compared with c-Si and Ag references. The c-Si (n) substrate showed a WF at 4.22 eV. After the deposition of the HTO films, the WF increased to values between 4.40 and 4.42 eV, depending on the film thickness. Figure 3b shows the SPVresponse after illumination. The WF moves back to ≈ 4.22 eV, which corresponds to the WF of the c-Si(n) substrate. This change indicates a realignment at the interface, possibly leading to a flat band state after illumination.[36]

© 2025 The Author(s). Advanced Materials Interfaces published by Wiley-VCH GmbH

21967350, 0, Downloaded from https://advanced.onlinelibrary.wiley.com/doi/10.1002/admi.202500083 by Cochrane France, Wiley Online Library on [20/05/2025]. See the Terms and Conditions (https://onlinelibrary.wiley.com/terms-and-conditions) on Wiley Online Library for rules of use; OA articles are governed by the applicable Creative Commons License

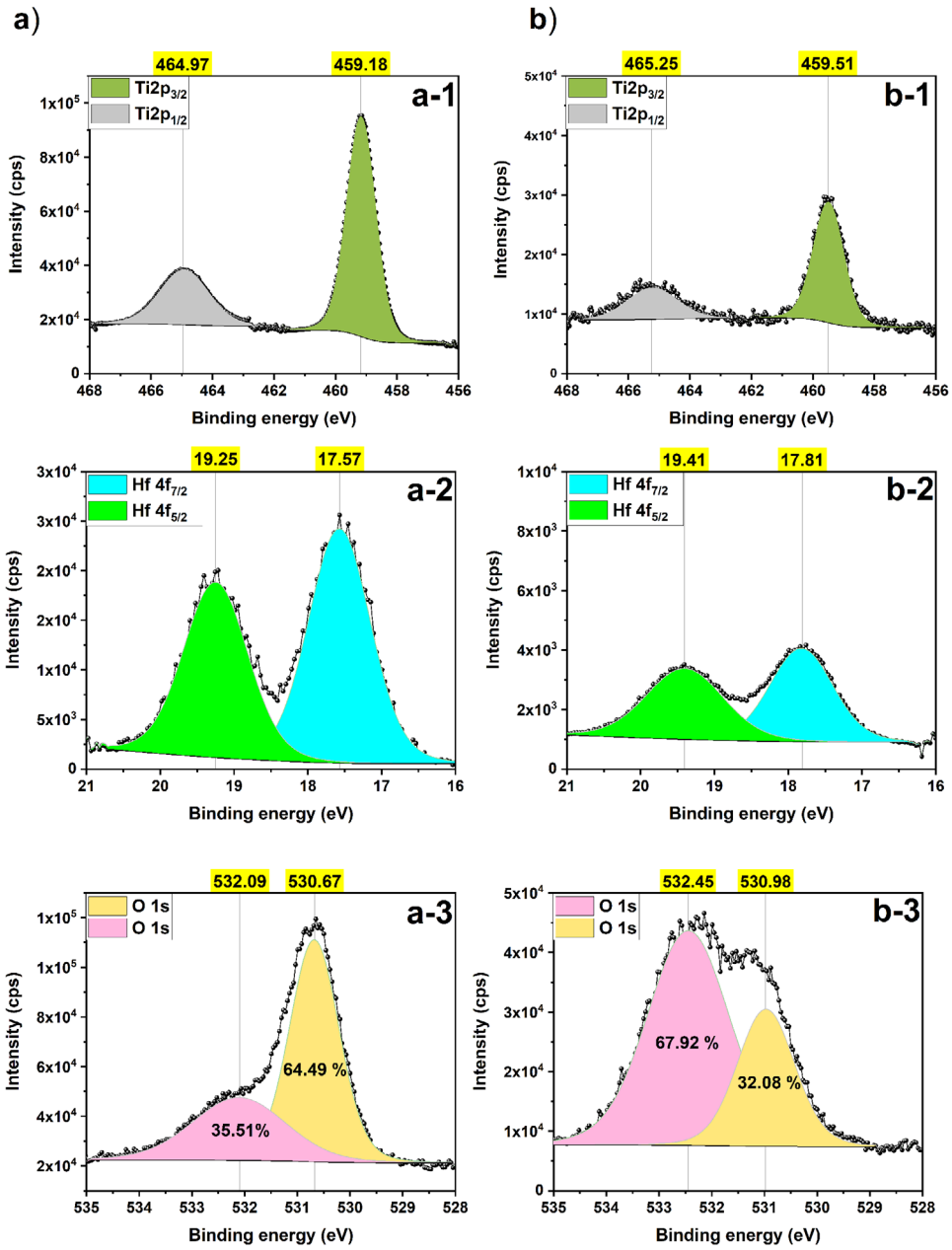

Figure 1. Core-level XPS spectra of Ti 2p, Hf 4f, and O 1s for HTO films: a) bulk HTO-10C, b) HTO-1C at the c-Si interface.

2.2.3. Energy Levels

The valence band position was further investigated using XPS to estimate the band offset at the c-Si(n)/HTO heterointerface. Three XPS spectra were collected to analyze the valence band maximum (VBM): one for a thicker HTO layer (10 cycles, ≈7 nm), one for an ultrathin HTO layer (one supercycle, <1 nm) to examine the interface characteristics, and one for a cleaned silicon substrate as a baseline reference. The VBM positions were determined by fitting the valence band edge using the "Edge Down" background type in CasaXPS,[37] allowing for precise extrapolation from the linear region near the edge.

Kraut et al method is used to calculate the valence band offset (VBO) using the Equation (1):[38–40]

$$VBO = E^{(b)}_{VBM} - E^{(a)}_{VBM} + V_{bb} \quad (1)$$

Here, $E^{(a)}_{VBM}$ and $E^{(b)}_{VBM}$ represent the valence band maximum (VBM) energies of c-Si(n) and HTO, respectively, and V_{bb} is the band bending at the interface. The bend bending V_{bb} can be determined using the following Equation (2):

$$V_{bb} = \left(E^{a}_{CL} - E^{a}_{CL}(i)\right) + \left(E^{b}_{CL}(i) - E^{b}_{CL}\right) \quad (2)$$

© 2025 The Author(s). Advanced Materials Interfaces published by Wiley-VCH GmbH

21967350, 0, Downloaded from https://advanced.onlinelibrary.wiley.com/doi/10.1002/admi.202500083 by Cochrane France, Wiley Online Library on [20/05/2025]. See the Terms and Conditions (https://onlinelibrary.wiley.com/terms-and-conditions) on Wiley Online Library for rules of use; OA articles are governed by the applicable Creative Commons License

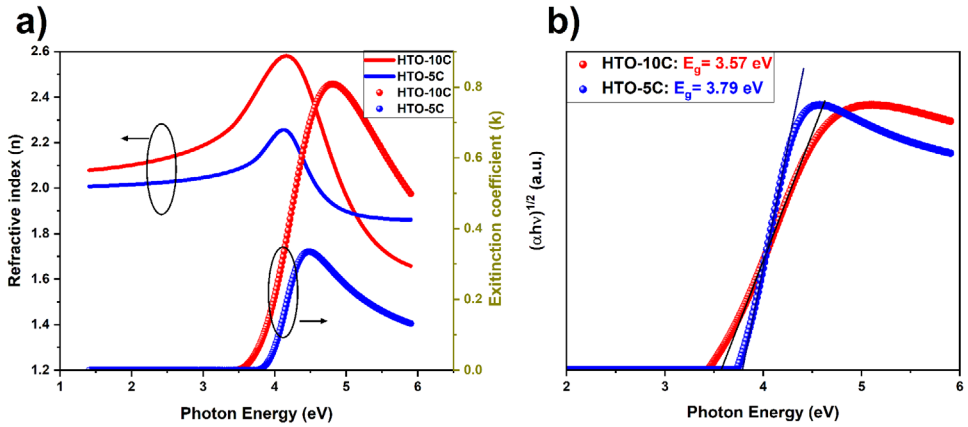

Figure 2. a) simulated n,k values; b) Tauc plot for a indirect bandgap material for HTO-5C and HTO-10C on c-Si(n).

Here, E^{a}_{CL} and E^{b}_{CL} represent the core level energies of bulk c-Si(n) and HTO respectively, while $E^{a}_{CL}(i)$ and $E^{b}_{CL}(i)$ are the core level energies at the heterointerface c-Si(n)/HTO. To reliably extract information about the core levels at the interface, the HTO film should ideally be ultrathin (i.e., much thinner than the mean free path of the photoelectrons) to allow the simultaneous collection of data from the HTO layer and the underlying c-Si substrate. The Fermi level was defined as the reference point at 0 eV, with binding energies below this level treated as negative values.

Figure 4a shows the VBM positions of HTO bulk, c-Si(n) bulk and c-Si(n)/HTO interface. The VBM of the thick HTO layer was positioned at 3.5 eV relative to the Fermi level. At the interface, the contributions from the HTO film and the underlying silicon substrate are clear, with a stronger influence from the c-Si substrate, resulting in a VBM position of ≈0.64 eV. The VBM of n-type bulk c-Si was determined to be ≈ 0.78 eV. Figure 4b shows the core level spectra for the overall HTO layer and c-Si(n)/HTO interface. The Ti $2p_{3/2}$ core level of the HTO layer is situated at 459.18 eV, shifting to 459.51 eV at the interface. The Si 2p core level of the c-Si substrate also shifts from 99.37 eV in the bulk to 99.47 eV at the interface. Based on these deviations, the calculated band bending (V_{bb}) is approximately 0.23 eV. These shifts in core levels and band bending can be attributed to interfacial fixed charges and dipole formation at the HTO/c-Si(n) interface. The presence of interfacial oxygen-related defects may contribute to the built-in dipole. In addition, the observed shift in the work function after illumination, as shown in Figure 3b, supports the hypothesis that charge redistribution occurs at the interface. This effect can be attributed to the generation of minority carriers under illumination, which contribute to interfacial charge rearrangement, partially realigning the bands at the interface as shown in Figure S5 (Supporting Information).

The CBO can also be estimated using the VBO and the difference in bandgaps (E_g) between the HTO and c-Si according to the following Equation (3):

$$\mathrm{CBO} = (E_g^{(b)} - E_g^{(a)}) + \mathrm{VBO} \quad (3)$$

Here, $E_g^{(a)}$ and $E_g^{(b)}$ are the bandgaps of c-Si and HTO, respectively. In this study, the bandgap of c-Si is taken as 1.12 eV, and that of HTO is 3.79 eV, which is consistent with the results obtained from ellipsometry measurements.

From the results, the calculated VBO is -2.95 eV, while the CBO is – 0.28 eV.

We can deduce from the above analyses the band structure of the c-Si/HTO contact. **Figure** 5a shows the energy levels of bulk

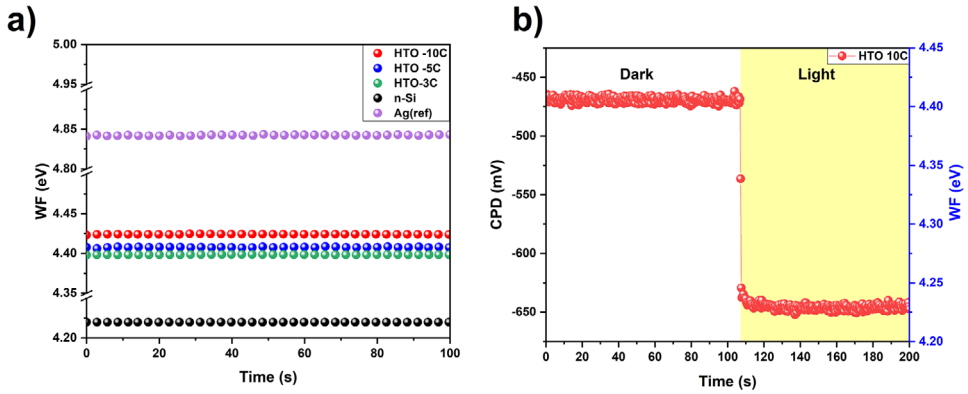

Figure 3. a) Steady-state dark work function of Ag reference, clean n-type c-Si and HTO films of different thicknesses (HTO-3C, HTO-5C and HTO-10C) recorded for 100 sec. using a Kelvin probe; b) Surface photovoltage (SPV) results illustrating the change in work function before and after illumination.

© 2025 The Author(s). Advanced Materials Interfaces published by Wiley-VCH GmbH

21967350, 0, Downloaded from https://advanced.onlinelibrary.wiley.com/doi/10.1002/admi.202500083 by Cochrane France, Wiley Online Library on [20/05/2025]. See the Terms and Conditions (https://onlinelibrary.wiley.com/terms-and-conditions) on Wiley Online Library for rules of use; OA articles are governed by the applicable Creative Commons License

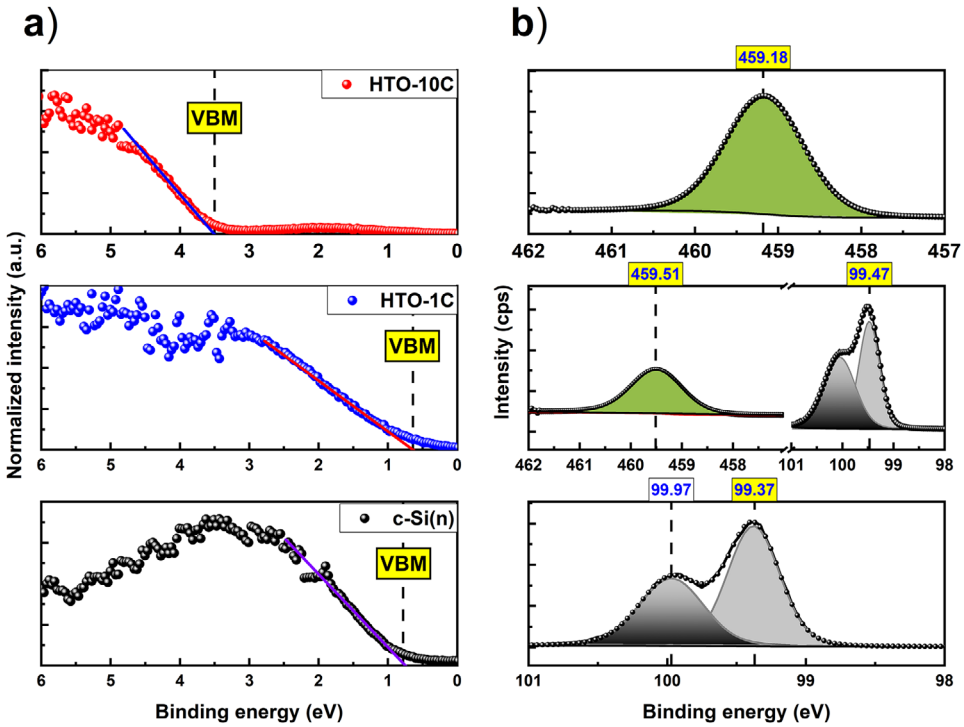

Figure 4. a) Valence band spectra for c-Si(n), the c-Si(n)/HTO interface, and bulk HTO; b) Core-level spectra showing Si 2p for c-Si(n), Ti 2p and Si 2p at the interface, and Ti 2p far from the interface.

c-Si and HTO separately, where the Fermi level of c-Si(n) is positioned at 4.22 eV, and the WF of HTO is positioned at 4.42 eV as determined by the KP measurement in Figure 3a. Here, 0 eV corresponds to the vacuum level.

Figure 5b shows the band alignment of the c-Si(n)/HTO heterointerface, where the Fermi levels align at 4.42 eV. The CBO was negative, indicating a type-II heterointerface with a small cliff-like CBO. This configuration facilitates the transport of electrons from the silicon conduction band to HTO. The high VBO acts as a reflector for holes, enabling the application of HTO as a selective contact for electrons.

2.3. Contact Resistivity Optimization

To assess the selectivity and contact resistivity of the materials, transmission line measurements (TLM) were conducted on the c-Si(n)/HTO-xC/Al and c-Si(p)/HTO-xC/Al configurations, as shown in **Figure 6**a. For the n-type c-Si(n) configuration, the super-cycles of HTO deposition were varied between 1 and 5.

The I-V characteristics of the p-type silicon configuration demonstrated a non-linear behavior, giving diode-like characteristics. As a result, HTO appears non-hole selective. For n-type configurations, the I-V curves show a linear behaviour for all samples, as shown in Figure 6c for the HTO-4C sample. The other samples with supercycles of 1, 2, 3 and 5 also showed linear behavior for all film thicknesses. The contact resistivity was extracted from the TLM measurements, using pad spacings ranging from 100 to 500 µm, as shown in Figure 6d.The best contact resistivity of ≈15.6 mΩ·cm^2 was obtained for the HTO-4C sample.

Our results reveal that the HTO layer provides an effective electron-selective contact for n-type silicon, achieving low contact resistivity without the need for additional interlayers. This clearly distinguishes this study from other studies of TiO_2-based selective contacts, which often include materials such as Ca or LiF between TiO_2 and Al to improve the performance.[19,21] Although these intermediate layers can improve the overall device behavior, they confound the precise origin of selectivity, making it unclear whether the observed effects originate from TiO_2, the intermediate layer, or their combination influence. In our case, the clear linear I-V characteristics of the n-type configuration and the nonlinear behavior of the p-type configuration directly confirm the electron selectivity of HTO, which can be attributed to a favorable band alignment at the c-Si(n)/HTO interface, where the low conduction band offset facilitates efficient electron extraction while blocking holes.

A proof of concept for functional solar cells was realised using HTO-4C as an electron selective contact on the rear of n-type silicon.In this configuration, the junction was formed on the front side by rapid thermal diffusion of boron to achieve the forward junction. The schematic diagram of the solar cells and the I-V characteristic are given in Figures S7 and S8 (Supporting Information). As shown in Figure S7 (Supporting Information), the I-V characteristics of the devices were obtained before and after the deposition of HTO-4C layer at the c-Si(n)/metal interface. Before the incorporation of HTO, the solar cell exhibited an extremely high series resistance, resulting in an open-circuit voltage (V_{oc}) of 443 mV, a fill factor (FF) of 25%, and a

© 2025 The Author(s). Advanced Materials Interfaces published by Wiley-VCH GmbH

21967350, 0, Downloaded from https://advanced.onlinelibrary.wiley.com/doi/10.1002/admi.202500083 by Cochrane France, Wiley Online Library on [20/05/2025]. See the Terms and Conditions (https://onlinelibrary.wiley.com/terms-and-conditions) on Wiley Online Library for rules of use; OA articles are governed by the applicable Creative Commons License

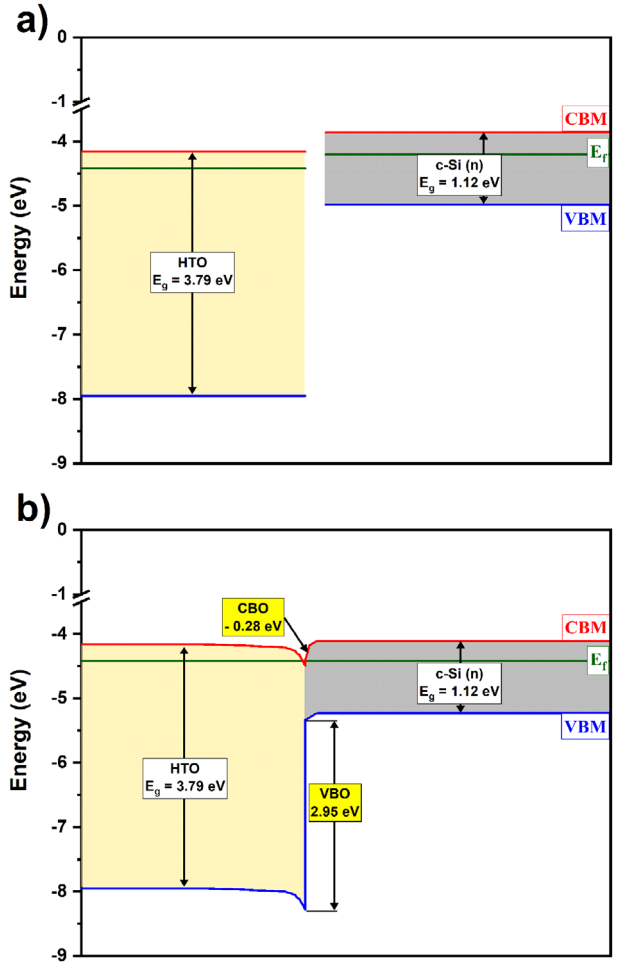

Figure 5. a) Energy levels of the individual materials (c-Si(n) and HTO) with respect to the vacuum level; b) Band alignment at the c-Si(n)/HTO interface, illustrating valence and conduction band offsets.

power conversion efficiency (PCE) of only 3.34%. After the incorporation of the HTO-4C film, a significant improvement in device performance was observed, with V_{oc} increasing to 565 mV, FF increasing to 62%, short circuit current density (J_{sc}) reaching ≈34 mA cm^{-2}, and efficiency increasing to 12.26%. These results clearly demonstrate the beneficial role of HTO films in improving all key solar cell performance parameters, despite the non-optimized device architecture. The relatively low V_{oc} observed in the device can be attributed to the modest passivation on both sides of the wafer. The front-side junction was fabricated by rapid thermal diffusion of boron without the application of a passivation layer such as Al_2O_3, which likely resulted in significant surface recombinations. In addition, some of the boron atoms introduced during diffusion may not have been fully activated. This is due to the short annealing time of only 5 s. A longer thermal treatment is typically used to ensure complete dopant activation and minimize recombination losses in high efficiency solar cells with heavily doped p^{++} emitters.[41] On the backside, injection level-dependent minority carrier lifetime measurements on c-Si(n) wafers with double-sided HTO-4C deposition, shown in the supplementary material (Figure S9, Supporting Information), indicate an extracted lifetime of ≈ 140 µs at 1 × 10^{15} cm^{-3} excess carrier density. This relatively modest lifetime highlights the need for further investigations on passivation strategies to minimize recombination losses and to fully exploit the potential of HTO as an electron-selective passivating contact. One promising direction to improve passivation quality would be to replace the titanium precursor with a chloride-based precursor during ALD growth of HTO, as demonstrated in previous studies on aluminum titanium oxide (ATO), where Cl^- incorporation significantly improves the passivation quality.[20–22] Future improvements could also focus on texturing the silicon for more effective light management and incorporating dopant-free hole-selective contacts to further boost the device performance.

3. Conclusion

This study provides an in-depth investigation of the chemical, electronic, and interfacial properties of HTO thin films on n-type c-Si substrates and establishes their potential as effective selective contacts for Si-based optoelectronic devices. The films were deposited by low-temperature ALD, a process compatible with temperature-sensitive applications and scalable toward large-scale engineering. This low-temperature process ensures a minimal thermal budget, making it suitable for advanced photovoltaic technologies.

Using X-ray photoelectron spectroscopy (XPS), we characterized the valence and conduction band offsets at the c-Si/HTO heterointerface, revealing a type II band alignment with a valence band offset (VBO) of 2.95 eV and a cliff-like conduction band offset (CBO) of ≈ -0.28 eV. This band alignment facilitates efficient electron transport from silicon to HTO while effectively blocking hole transport, thus meeting the requirements for selective contact functionality.

Electrical characterization via transmission line measurements (TLM) demonstrated a contact resistivity as low as 15.6 mΩ·cm^2 for the HTO-4C configuration with an Al metal contact, highlighting its high performance without needing intermediate layers, such as Ca or LiF. A proof-of-concept solar cell with HTO-4C between the aluminum and c-Si(n) showed a significant improvement in performance, with an increase in the open circuit voltage (V_{oc}) from 443 to 565 mV and an increase in the efficiency from 3.34% to 12.26%.

These results highlight the potential of HTO thin films for integration into silicon photovoltaic and optoelectronic applications, offering a favorable energy band structure and superior charge carrier selectivity. Future research should focus on optimizing the interface quality, reducing oxygen-related defects and integrating these selective contacts instead of junction into complete silicon devices based on transition-metal oxides.

4. Experimental Section

Synthesis of HTO Thin Films: Double-side polished n- or p-type float-zone (FZ) silicon wafers with a resistivity of 1–5 Ω·cm and a thickness of ≈250 µm were used for the deposition of $Hf_xTi_{1-x}O_y$ (HTO) films. The wafers were first cleaned with 5% HF solution, rinsed in deionized water, and treated with ozone (O_3) for 15 min. The resulting oxide was then removed with 5% HF. The samples were then rinsed in deionized water and dried under nitrogen (N2) flow.

© 2025 The Author(s). Advanced Materials Interfaces published by Wiley-VCH GmbH

21967350, 0, Downloaded from https://advanced.onlinelibrary.wiley.com/doi/10.1002/admi.202500083 by Cochrane France, Wiley Online Library on [20/05/2025]. See the Terms and Conditions (https://onlinelibrary.wiley.com/terms-and-conditions) on Wiley Online Library for rules of use; OA articles are governed by the applicable Creative Commons License

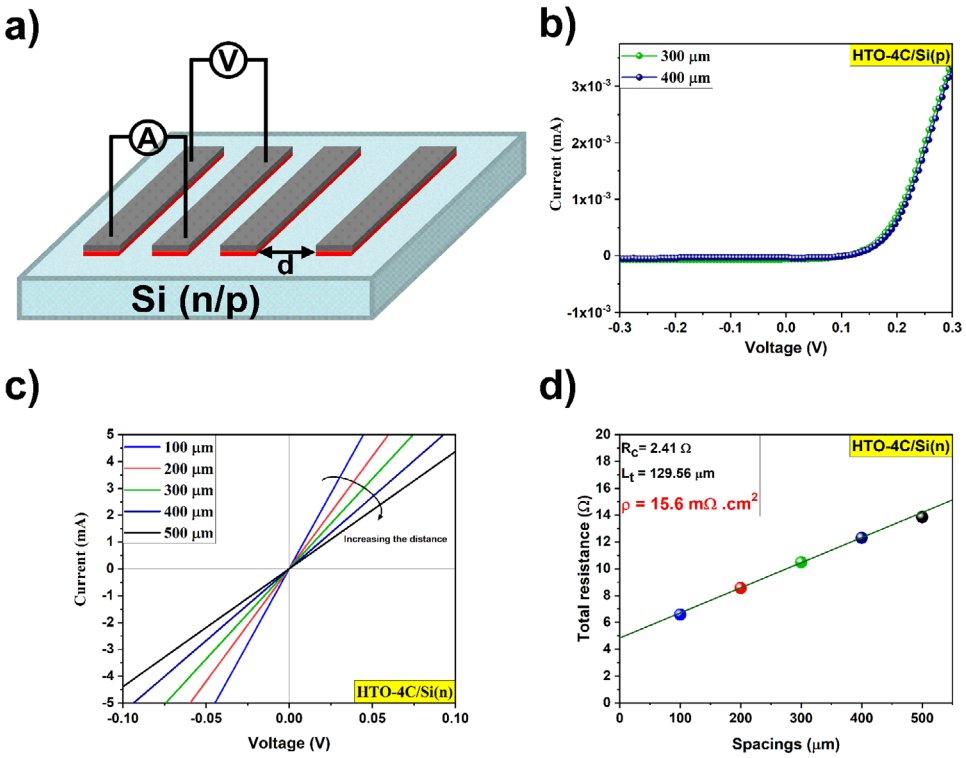

Figure 6. a) Illustration of the TLM measurement configuration. b) *I–V* curves for HTO-4C on c-Si(p). (c) *I–V* curves for HTO-4C on c-Si(n) with varying pad spacings. d) Total resistance as a function of electrode spacing.

The deposition of HTO films was carried out using an Ultratech Fiji F200 atomic layer deposition (ALD) system. Tetrakis(dimethylamido)hafnium(IV) (TDMAH) was used as the Hf precursor, Tetrakis(dimethylamido)titanium(IV) (TDMAT) as the Ti precursor, and deionized water (H_2O) as the oxidizing agent. The Hf and Ti precursors were heated to 75° C, while the water was kept at room temperature. During this process, the temperature of the chuck and the chamber were kept at 75 °C. The chuck and chamber temperature were selected based on recent studies on the deposition of aluminum-titanium oxide alloys, which demonstrated optimal film quality.[20–22]

The deposition was performed using a sequence of supercycles. Each supercycle consisted of one cycle of Hf precursor followed by the oxidant, and then five cycles of the Ti precursor followed by the oxidant. These supercycles were repeated multiple times to evaluate the effect of film thickness on selectivity and contact resistance. In this manuscript, HTO films are referred to as HTO-xC, where "x" refers to the number of supercycles completed.

Contact Engineering: For contact engineering, 1 mm x 5 mm transfer length method (TLM) pads were fabricated on p-type and n-type c-Si substrates, with pad spacings ranging from 100 to 500 µm.[42] Initially, HTO films were deposited on clean silicon wafers. A 200 nm thick aluminium (Al) layer was then evaporated over the HTO film surface. The lithographic patterns of the TLM pads were defined on the aluminum layer using AZ5214 positive photoresist, which was exposed to UV light using an UV EVG 620 photomask aligner. Once the lithography process was completed, the aluminum film was etched with an aluminum etching solution. The exposed HTO films were then etched by reactive ion etching (RIE) using a mixture of SF_6 and Ar gases at a chamber pressure of 50 mTorr and an RF power of 100 W. Finally, the contact resistivity as a function of HTO thickness was investigated by measuring the *I–V* characteristics using a Keithley 2400 source meter.

Characterization: The surface morphology and roughness of the films were characterised by atomic force microscopy (AFM) (AFM Bruker Dimension Icon) (Figure S1, Supporting Information). The chemical environment of the HTO thin films was analyzed by X-ray electron spectroscopy (XPS) using a hemispherical energy analyzer (EA15-HP) equipped with an aluminum monochromator (incident energy of 1486 eV). Pure gold metal (Au 4f at 84 eV) was used as a reference. The optical properties and thickness of the films were investigated by spectroscopic ellipsometry using a HORIBA Uvisel Lt M200 FGMS (210–880 nm). Kelvin probe (KP) and SPV measurements were performed using a single component setup (APS03, KP Technology).[43,44] Tip calibration was performed by determining the contact potential difference (CPD) with a silver reference. For SPV measurements, illumination was provided by a quartz tungsten halogen light source with a maximum irradiance of ≈19 mW cm^{-2}. Finally, the contact resistance as a function of HTO thickness and the efficiency of the solar cells were investigated by measuring the *I–V* characteristics using a Keithley 2400 source meter and AM1.5 solar simulator.

Supporting Information

Supporting Information is available from the Wiley Online Library or from the author.

Acknowledgements

The present project was financed by the ANR Exosil-Exotic Silicon: Silicon Clathrate Films (project-ANR-22-CE50-0025) and supported by the Nanolyon platform, a member of the French national network CNRS-RENATECH+. The authors acknowledge the Consortium Lyon Saint-Etienne de Microscopie (CLYM, FED 4092) for access to the microscopes.

Conflict of Interest

The authors declare no conflict of interest.

© 2025 The Author(s). Advanced Materials Interfaces published by Wiley-VCH GmbH

21967350, 0, Downloaded from https://advanced.onlinelibrary.wiley.com/doi/10.1002/admi.202500083 by Cochrane France, Wiley Online Library on [20/05/2025]. See the Terms and Conditions (https://onlinelibrary.wiley.com/terms-and-conditions) on Wiley Online Library for rules of use; OA articles are governed by the applicable Creative Commons License

Data Availability Statement

The data that support the findings of this study are available from the corresponding author upon reasonable request.

Keywords

atomic layer deposition, band alignment, photovoltaic, selective contacts

Received: January 28, 2025
Revised: March 31, 2025
Published online:

[1] M. A. Green, *Sol. Energy Mater. Sol. Cells* **2015**, *143*, 190.
[2] H. Lin, M. Yang, X. Ru, G. Wang, S. Yin, F. Peng, C. Hong, M. Qu, J. Lu, L. Fang, C. Han, P. Procel, O. Isabella, P. Gao, Z. Li, X. Xu, *Nat. Energy* **2023**, *8*, 789.
[3] T. G. Allen, J. Bullock, X. Yang, A. Javey, S. De Wolf, *Nat. Energy* **2019**, *4*, 914.
[4] A. Prasetio, R. R. Pradhan, P. Dally, M. Ghadiyali, R. Azmi, U. Schwingenschlögl, T. G. Allen, S. De Wolf, *Adv. Energy Mater.* **2024**, *14*, 2303705.
[5] N. L. Chang, G. K. Poduval, B. Sang, K. Khoo, M. Woodhouse, F. Qi, M. Dehghanimadvar, W. M. Li, R. J. Egan, B. Hoex, *Prog. Photovolt. Res. Appl.* **2023**, *31*, 414.
[6] L. Li, G. Du, Y. Lin, X. Zhou, Z. Gu, L. Lu, W. Liu, J. Huang, J. Wang, L. Yang, S.-T. Zhang, D. Li, *Cell Rep. Phys. Sci.* **2021**, *2*, 100684.
[7] W. Ahmad, S. Tahir, A. Ali, K. Mahmood, *Ceram. Int.* **2023**, *49*, 2821.
[8] E. Aydin, J. Troughton, M. De Bastiani, E. Ugur, M. Sajjad, A. Alzahrani, M. Neophytou, U. Schwingenschlögl, F. Laquai, D. Baran, S. De Wolf, *ACS Appl. Energy Mater.* **2018**, *1*, 6227.
[9] S. Liu, R. Liu, Y. Chen, S. Ho, J. H. Kim, F. So, *Chem. Mater.* **2014**, *26*, 4528.
[10] G. Bartholazzi, M. M. Shehata, D. H. Macdonald, L. E. Black, *J. Vac. Sci. Technol. A* **2023**, *41*, 022402.
[11] E. R. Costals, G. Masmitjà, E. Almache, B. Pusay, K. Tiwari, E. Saucedo, C. J. Raj, B. C. Kim, J. Puigdollers, I. Martin, C. Voz, P. Ortega, *Mater. Adv.* **2022**, *3*, 337.
[12] T. Zhang, Md. A. Hossain, C.-Y. Lee, Y. Zakaria, A. A. Abdallah, B. Hoex, *Appl. Phys. Lett.* **2018**, *113*, 262102.
[13] J. Ding, Y. Zhou, G. Dong, M. Liu, D. Yu, F. Liu, *Prog. Photovolt. Res. Appl.* **2018**, *26*, 974.
[14] M. Liu, Y. Zhou, G. Dong, W. Wang, J. Wang, C. Liu, F. Liu, D. Yu, *Sol. Energy Mater. Sol. Cells* **2019**, *200*, 109996.
[15] Z. Li, A. Xie, Q. Nong, Y. Sun, H. Cai, Z. Chen, J. He, P. Gao, *Small Sci.* **2024**, *4*, 2400168.
[16] N. Beyraghi, M. C. Sahiner, O. Oguz, S. Yerci, *ACS Appl. Mater. Interfaces* **2024**, *16*, 16950.
[17] Y. Liu, L. Zhang, H. Cheng, X. Song, S. Zhong, L. Shi, Z. Huang, *Adv. Mater. Interfaces* **2022**, *9*, 2201512.
[18] J. Bullock, P. Zheng, Q. Jeangros, M. Tosun, M. Hettick, C. M. Sutter-Fella, Y. Wan, T. Allen, D. Yan, D. Macdonald, S. De Wolf, A. Hessler-Wyser, A. Cuevas, A. Javey, *Adv. Energy Mater.* **2016**, *6*, 1600241.
[19] Y. Liu, B. Sang, Md. A. Hossain, K. Gao, H. Cheng, X. Song, S. Zhong, L. Shi, W. Shen, B. Hoex, Z. Huang, *Sol. Energy* **2021**, *228*, 531.
[20] M. M. Shehata, D. H. Macdonald, L. E. Black, *ACS Appl. Mater. Interfaces* **2023**, *15*, 46504.
[21] M. M. Shehata, P. Phang, R. Basnet, Y. Yin, F. Kremer, G. Bartholazzi, G. G. Andersson, D. H. Macdonald, L. E. Black, *Sol. RRL* **2022**, *6*, 2200550.
[22] M. M. Shehata, G. Bartholazzi, D. H. Macdonald, L. E. Black, *Adv. Energy Mater.* **2023**, *13*, 2300251.
[23] Y. Hong, X. Kuang, Y. Chen, Y. Xiao, Z. Liang, *Phys. Status Solidi A* **2024**, *221*, 2400387.
[24] R. A. Bennett, J. S. Mulley, M. Basham, M. Nolan, S. D. Elliott, P. A. Mulheran, *Appl. Phys. A* **2009**, *96*, 543.
[25] P. Krishnan, M. Liu, P. A. Itty, Z. Liu, V. Rheinheimer, M.-H. Zhang, P. J. M. Monteiro, L. E. Yu, *Sci. Rep.* **2017**, *7*, 43298.
[26] T. Cottre, M. Fingerle, M. Kranz, T. Mayer, B. Kaiser, W. Jaegermann, *Adv. Mater. Interfaces* **2021**, *8*, 2002257.
[27] M. J. Jackman, A. G. Thomas, C. Muryn, *J. Phys. Chem. C* **2015**, *119*, 13682.
[28] H. Wang, P. Wu, X. F. Li, S. Chen, S. P. Zhang, B. B. Song, *Appl. Surf. Sci.* **2011**, *257*, 3440.
[29] N. Kumar, B. P. A. George, H. Abrahamse, V. Parashar, S. S. Ray, J. C. Ngila, *Sci. Rep.* **2017**, *7*, 9351.
[30] S. Jain, J. Shah, N. S. Negi, C. Sharma, R. K. Kotnala, *Int. J. Energy Res.* **2019**, *43*, 4743.
[31] A. Deshpande, R. Inman, G. Jursich, C. Takoudis, *Microelectron. Eng.* **2006**, *83*, 547.
[32] A. Herrera-Gomez, F. S. Aguirre-Tostado, M. A. Quevedo-Lopez, P. D. Kirsch, M. J. Kim, R. M. Wallace, *J. Appl. Phys.* **2008**, *104*, 103520.
[33] M. A. Martínez-Puente, P. Horley, F. S. Aguirre-Tostado, J. López-Medina, H. A. Borbón-Nuñez, H. Tiznado, A. Susarrey-Arce, E. Martínez-Guerra, *Mater. Sci. Eng. B* **2022**, *285*, 115964.
[34] F. Wooten, *Optical Properties of Solids*, Elsevier Inc, New York **1972**.
[35] P. Makuła, M. Pacia, W. Macyk, *J. Phys. Chem. Lett.* **2018**, *9*, 6814.
[36] M. Daboczi, *Origin of Charge Carrier Recombination Losses in Perovskite-Based Solar Cells Revealed by Interfacial Energetics and Surface Photovoltage*, Imperial College London, London **2020**.
[37] N. Fairley, V. Fernandez, M. Richard-Plouet, C. Guillot-Deudon, J. Walton, E. Smith, D. Flahaut, M. Greiner, M. Biesinger, S. Tougaard, D. Morgan, J. Baltrusaitis, *Appl. Surface Sci. Adv.* **2021**, *5*, 100112.
[38] D. O. Scanlon, C. W. Dunnill, J. Buckeridge, S. A. Shevlin, A. J. Logsdail, S. M. Woodley, C. R. A. Catlow, M. J. Powell, R. G. Palgrave, I. P. Parkin, G. W. Watson, T. W. Keal, P. Sherwood, A. Walsh, A. A. Sokol, *Nat. Mater.* **2013**, *12*, 798.
[39] E. A. Kraut, R. W. Grant, J. R. Waldrop, S. P. Kowalczyk, *Phys. Rev. Lett.* **1980**, *44*, 1620.
[40] A. Santoni, F. Biccari, C. Malerba, M. Valentini, R. Chierchia, A. Mittiga, *J. Phys. Appl. Phys.* **2013**, *46*, 175101.
[41] Q. Wang, K. Guo, L. Yuan, L. Li, H. Peng, B. Li, A. Wang, L. Zhang, W. Wu, J. Ding, N. Yuan, *Sol. Energy Mater. Sol. Cells* **2023**, *253*, 112231.
[42] G. K. Reeves, H. B. Harrison, *IEEE Electron Device Lett.* **1982**, *3*, 111.
[43] A. K. Bharwal, R. Vollondat, C. Tamin, S. Roques, J. Bartringer, D. Stoeffler, C. Chevalier, A. Dinia, A. Slaoui, T. Fix, *ACS Appl. Energy Mater.* **2024**, *7*, 8554.
[44] A. K. Bharwal, J. P. Briggs, C. Tamin, M. Hanauer, R. Vollondat, J. Bartringer, S. Roques, C. Chevalier, A. Dinia, R. T. Collins, A. Slaoui, T. Fix, *ACS Appl. Energy Mater.* **2025**, *8*, 1752.

© 2025 The Author(s). Advanced Materials Interfaces published by Wiley-VCH GmbH

21967350, 0, Downloaded from https://advanced.onlinelibrary.wiley.com/doi/10.1002/admi.202500083 by Cochrane France, Wiley Online Library on [20/05/2025]. See the Terms and Conditions (https://onlinelibrary.wiley.com/terms-and-conditions) on Wiley Online Library for rules of use; OA articles are governed by the applicable Creative Commons License